PROCEEDINGS, 42nd Workshop on Geothermal Reservoir Engineering
Stanford University, Stanford, California, February 13-15, 2017
SGP-TR-212

Role of Fluid Injection Pressure in Inducing Seismicity

Zoheir Khademian, Masami Nakagawa, Ryan Garvey, and Ugur Ozbay

Colorado School of Mines, Golden CO.

zoheirkhademian@gmail.com

Keywords: Induced seismicity, seismic energy, injection pressure, deconfinement, wastewater disposal, enhanced geothermal systems

ABSTRACT

Seismicity triggered by the injection of fluid into fractured ground is one of the most pressing, yet difficult to address, rock mechanics issues facing oil, natural gas, and geothermal projects today. This paper describes a numerical study conducted in the distinct element code UDEC to analyze the seismicity triggered by the injection of water into a single fault, presenting a simplified analogy for the injection process in deep wastewater disposal fields and enhanced geothermal systems. An energy-based analysis is developed for studying these unstable slip events by calculating the total kinetic energy released when conditions for seismic slip emerge. In this method, the stress distribution and the relative changes of the energy terms in the system are assessed before, during, and after slip has occurred along the discontinuity. Validation testing of this method is first performed by simulating a direct shear test with the distinct element code UDEC. A more realistic model of a finite fault imbedded in a rock mass is then developed to capture the role of fluid injection pressure in triggering seismic slip. The Continuously-Yielding and Mohr-Coulomb elastoplastic joint models are adopted for representing brittle and ductile discontinuity responses, respectively. A range of material and system parameters is selected to cover both stable and unstable slip conditions. Unstable slip is shown to cause a release of kinetic energy (i.e. seismicity) as more energy is made available in the system than can be stored or consumed through the failure process. The effects of raising the fluid pressure and initiating slip along the discontinuity is then studied. For each model, the radiated seismic energy is calculated from the total kinetic energy released during failure and used as a measure of the relative magnitudes of instability for the given conditions. Two cases of loaded faulting are studied: well-oriented and misoriented. The results show that for the case of a well-oriented fault, rapid increase of fluid pressure within a fault can trigger a self-propagating and unstable slip; this occurs even for the case of the ductile fault, although the magnitude of the radiated seismic energy increases dramatically as more brittle failure characteristics are assigned to the discontinuity. For the case of misoriented faults which are not critically loaded, the rate of increasing injection pressure does not trigger seismicity under a certain pressure. At this fluid pressure, the shear strength of the fault reaches to the level of the shear stresses acting on the fault and the pressure rate comes into effect. These results can help drive future studies into the maximum injection rate and allowable downhole pressure increases before seismic slip is likely to be initiated.

1. INTRODUCTION

Settings encountering induced seismicity experience tremors precipitated by the stress redistribution and resultant changes in the strain energy stored in the Earth's crust due to man-made activities. These activities include mining and tunneling (Garvey and Ozbay 2013), unconventional oil and gas reservoirs (Rutqvist et al. 2013), enhanced geothermal systems (Evans et al. 2012; Bakhsh, et al. 2016), and deep well injection fields (Zhang et al. 2013). The changes in stress patterns may emanate from underground excavations (Khademian et al. 2012), pore pressure perturbation (Karimi and Kazemi 2015; Karimi and Saidian 2015, Karimi et al. 2016) or change in the rock temperature (Bakhsh, et al. 2016, Nakagawa et al. 2016). The Earth reacts to the induced stresses and releases the accumulated strain energy through failure in different modes. Failures may occur in a stable, gradual manner or in an unstable, violent mode (Gu and Ozbay 2015). During both forms of failure, the strain energy accumulated in the system relaxes; however, during a stable failure, the stored energy is fully consumed by the plastic work. The accumulated strain energy due to the interseismic accumulation is not completely exhausted during an unstable failure and results in releasing some kinetic energy referred to as seismic energy.

Attempts have been made to study the conditions required to trigger seismicity, identify a seismic event, and estimate the timing and magnitude of these unstable events. Researchers have used high slip velocity, shear stress drop and shear failure as criteria to identify seismic events (McClure and Horne 2011). In order to calculate the seismic energy of an event, many researchers also calculated the magnitude of the seismic energy by relying on the seismic moment which is the product of the rupture length, shear modulus of the rock, and total shear displacement (Rutqvist et al. 2013).

This paper discusses a numerical methodology in which a seismic event is identified by directly calculating the magnitude of the kinetic energy that radiates if the conditions for instability emerge. Given the stress state, we calculate the energy available for failure, energy stored in the system, energy consumed by the failure, and finally the energy that is released during the unstable failure of the system. A numerical direct shear test is used to study instability in the energy framework and then the methodology is further extended for exploring seismicity along a finite fault in such settings as enhanced geothermal systems and deep wastewater disposal, characterized by fluid injection.

2. ENERGY BALANCE

Slip along a fault is accompanied by a transfer of energy within the surrounding rock mass. Khademian et al. (2016) employed the analytic solutions provided by Duvall and Stephenson (1965), Salamon (1984), and Cook (1966) for energy transfer in an elastic medium and compared the results against the calculation of the static energy terms in UDEC. This same approach was then extended to include the potential for inelastic deformations and a dissipative energy term for plastic work (W_p). Two sources of energy mainly drive shear slip: the work done by external or gravitational forces (ΔW) and the interseismic strain energy (ΔU) that has been stored in the footwall and hanging wall. The interseismic accumulation, or steady pre-slip deformation of rockmass surrounding the fault is stored as elastic strain energy. Seismic energy (W_k) radiates from the system when strain energy from the surrounding media cannot be fully consumed by plastic work (Salamon 1984). A static energy balance describes the transfer of energy, as shown in Eq. (1)

$$W_k = \Delta W - W_p - \Delta U \tag{1}$$

The DEM numerical scheme in UDEC allows the direct calculation of the dynamic term, W_k. UDEC uses an explicit time-marching where mechanical damping is adopted to reach a solution of static equilibrium for each model. The energy balance based on the kinetic terms in the system is governed by Equation 2 (Itasca, 2014) and U_k is the total kinetic energy of the system at a given time.

$$W_k = U_k + W_D \tag{2}$$

The damped work is a cumulative term that represents the sum of kinetic energy extracted by UDEC through mechanical damping of unbalanced gridpoint forces. The current kinetic energy is not cumulative so that it is near zero as the model reaches equilibrium and is high during simulated dynamic and/or unstable failure (Poeck et al. 2016). Section 3 examines the dynamic calculation of energy terms in UDEC by calculating the static energy transfers directly from the recorded changes in stresses and displacements within a simple model of shear slip.

3. MODELING SHEAR INSTABILITY

3.1 Energy Calibration

Cook (1965) presented a theoretical derivation of the energy terms during unstable rock failure using laboratory compression tests on cylindrical rock samples. These studies revealed that the kinetic energy released during failure depends profoundly on the stiffness of the loading machine platens. Using a box-spring system, Salamon (1974) and then (Rice 1983) showed that if the spring stiffness remains greater than the post-peak slope of the shear force-displacement curve of the box contact, stable slip occurs along the surface. By contrast, a spring with a relatively low stiffness leads to an unstable slip failure at the contact surface leading to radiation of some "seismic energy". The stiffness of the spring is comparable to the loading stiffness in the case of a geological fault, and therefore dictates the amount of energy that can be stored in the fault wall rocks. The accumulated strain energy may be partly consumed as plastic work during the slip and partly released in the form of a seismic event. The magnitude of this released energy can be quantified by comparing the post-peak stress versus displacement curve of the fault with that of the surrounding materials (Salamon, 1969). This section employs the direct shear test configuration (Gu and Ozbay 2015, Khademian, et al. 2016) and investigates the concept of instability in the framework of static and dynamic energy balance.

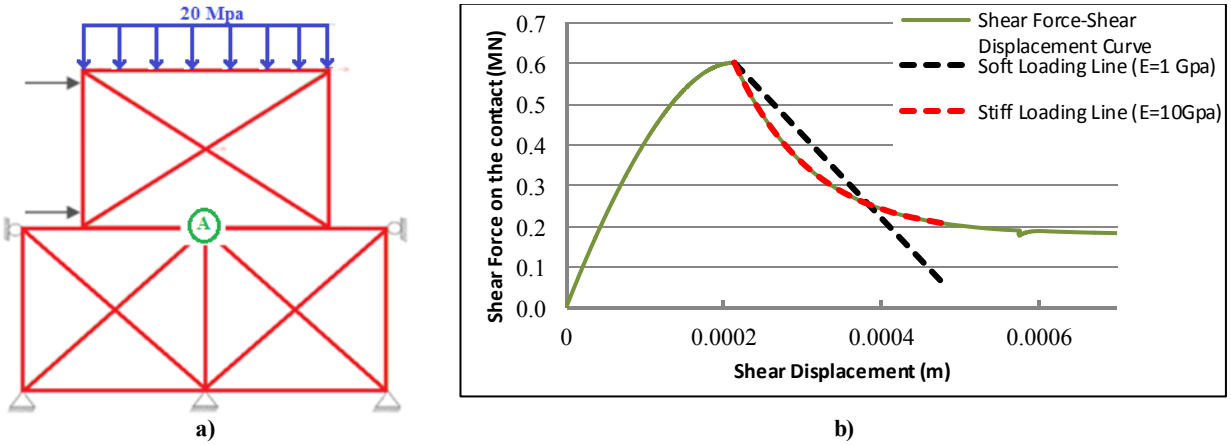

Figure 1: a) Numerical model for the direct shear test. b) The behavior of the discontinuity and loading systems during the slip in the direct shear test. Shear force-shear displacement curve at point A along with the loading stiffness lines. The solid purple line is the shear force-displacement curve along the discontinuity; the dashed black curve is the stiffer loading line with E=10GPa; the dashed red line is the softer loading line with E= 1GPa

This configuration is mainly adopted to identify the factors that have an influence on the magnitude of a seismic event. Figure 1 shows the direct shear test in which the number of meshes is deliberately reduced to decrease the shear failure localization and enable the comparison between the slope of the post peak and loading stiffness curves. Effects of shear localization and the number of meshes on the results of the direct shear test simulation are detailed in section 3.2. The shear test model comprises two rectangular blocks with each block being 0.15 m high. The top and bottom blocks have 0.2 m and 0.3 m widths, respectively and can be thought of as the simplified representation of the hanging wall and footwall of a fault in a geological setting. The interface between blocks, simulating an infinite fault, is modeled using a Continuously Yielding (CY) joint model with the brittle characteristics shown in Table 1. The CY joint model simulates the brittle behavior of joints consistent with a seismological slip-weakening fault. The loading conditions and model fixity are outlined in Figure 1a.

Table 1. Input parameters for the CY joint model in the direct shear test

Term	Value	Term	Value
Joint normal stiffness	50.0 GPa/m	Joint initial friction angle	34.0°
Joint shear stiffness	50.0 GPa/m	Joint roughness parameter	0.1 mm
Joint basic friction angle	5.0°	Cohesion	0.0

A constant horizontal velocity of 1 mm/s per simulation time is applied over the left side of the rock specimen. Figure 1b is the result of running two shear tests: one with the stiffer blocks and another one with the softer. The solid line is obtained from recording the shear force and shear displacement at point A in Figure1a. The dashed curves show the loading stiffnesses, which are functions of the dimensions and shear moduli of the blocks. Here, Young's modulus is changed to study the role of loading stiffness on instability. These stiffnesses are obtained through the procedure proposed by (Gu and Ozbay 2015). The black and red dashed curves represent soft and stiff loading systems with blocks of Young's moduli of 1 and 10 GPa, respectively. The slope of the loading line correlates with the stiffness of the system. Theoretically, the area below the dashed lines is ΔW denoting the energy available for the slip failure in each case and that of the solid line is W_p, the consumed energy throughout the slip.

Based on Equation 1 and the instability notion provided by Salamon (1976) and Cook (1983), the area between the solid and dashed lines is a representative of W_k, the seismic energy which is released when the conditions for instability are met (Khademian, et al. 2016). For the stiff loading system, the available energy is fully consumed and the block relaxation follows the same path as the shear slip. Therefore, near-zero seismic energy is expected as velocity loading is advanced so slowly that the only possible source of significant kinetic energy is the shear seismic energy, seismic energy due to shear slip. This is confirmed by the results listed in Table 2. For the soft loading system, the graphically calculated area between the black dashed line and the post peak curve is equivalent to 13.96 J, which is in agreement with the dynamic calculation of the released energy. The numerical results denote UDEC calculation of the damped work and current kinetic energy can be used to study unstable slip along a discontinuity.

Table 2: Comparison between analytic and numerical methods for slip failure.

Loading Stiffness	Seismic energy (J)		Difference %
	Graphical Calculation	Dynamic Calculation By UDEC	
Soft system	13.96	13.30	4.7
Stiff system	0.00	1.21e-3	~

As mentioned before, the number of meshes in the direct shear test shown Figure 1a was kept so low that the verification of energy terms was possible. However, a more realistic result demands a study on the number of meshes since the mesh size affects the shear failure localization and the simulated magnitude of the released seismic energy.

3.2 Shear failure localization

Shear failure of brittle faults is associated with the onset of localized inelastic deformation along the discontinuity. Localization depends on the stiffness of the surrounding rocks (Anderson, Fleck et al. 1990) and affects the average shear strength of a discontinuity. In numerical modeling of a crack under a shear force, the number of meshes along the simulated crack is crucial for grasping the shear failure localization. Our study on the effects of shear failure localization begins with a parametric study on the mesh sizes where the direct shear test model in Figure1a is discretized into finer meshes and the number of meshes in the model is increased systematically. Mesh size is seen to affect the average shear stress required to move the upper block to a point under which results are independent of the mesh sizes. Figure 2a shows the mesh independent model with 8840 meshes dividing the interface between the blocks into 70 contact elements. Two different loading systems are also applied for studying their relative impacts on shear failure localization: a stiff system with Young's modulus of 10 GPa and a soft system with Young's modulus of 1 GPa. Figure 3 a and b plot the recorded shear stress versus simulation time at 5 recorded contact areas (A, B, C, D, E) along the discontinuity for stiff and soft loading lines, respectively.

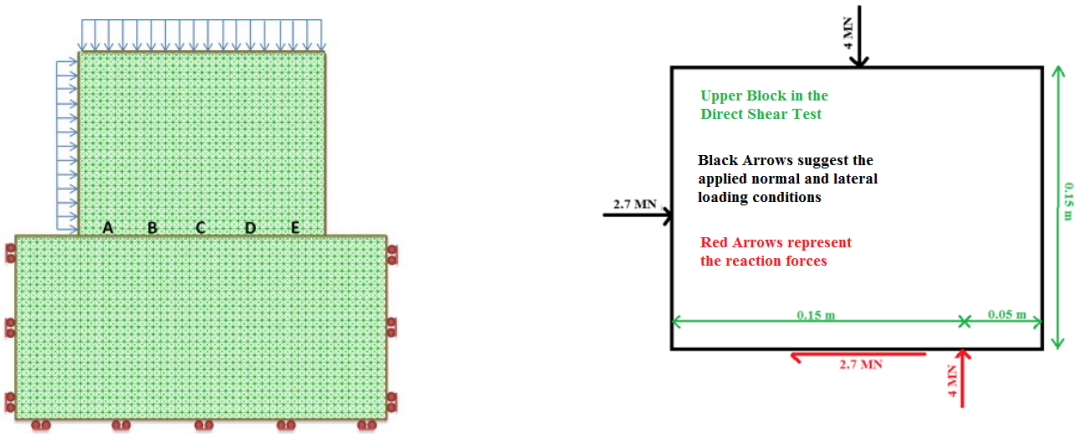

a) b)

Figure 2: a) UDEC model of the direct shear test with 8840 meshes dividing the interface into 70 contact elements. Contacts A to E are the control points specifying the location of recorded data on the model. b) Free body diagram of the upper block. The black arrows stand for the applied loads and red arrows show the reaction forces.

The average shear stress along the discontinuity is also recorded during the test via averaging the shear stress on the 70 contact elements along the crack. As shown in Figure 3, failure initiates at contact A and propagates all the way through the crack to contact E. This phenomenon can be explained via the free body diagram outlined in Figure2b. This diagram represents the resultant forces and the respective reaction forces acting on the upper block in the direct shear test at the point of shear failure. The highest normal stress is shown to be at contact D building the highest and lowest shear strength at contacts D and A, respectively. Note that in the model, the normal reaction loads are distributed along the contact with their maximum of 4 MN acting at the point specified in Figure2b. The characteristic curve for each individual contact area follows the one shown in Figure1b (Y axis in Figure 1b must be divided by the 0.1 length of contact A to yield shear stresses). The insignificant inconsistency between the peak shear strength of these five contact elements originates from the nonuniform normal stress concentration induced by the loading condition. The average shear stress that mainly governs the throughgoing slip shows a decrease in the overall peak strength of the crack in both systems in Figure 3. As failure originates at contact A, other contacts still climb causing a lower average shear stress along the discontinuity. However, for blocks with lower Young's modulus, this reduction in strength is more remarkable and show that stiff systems are less affected by the shear failure localization.

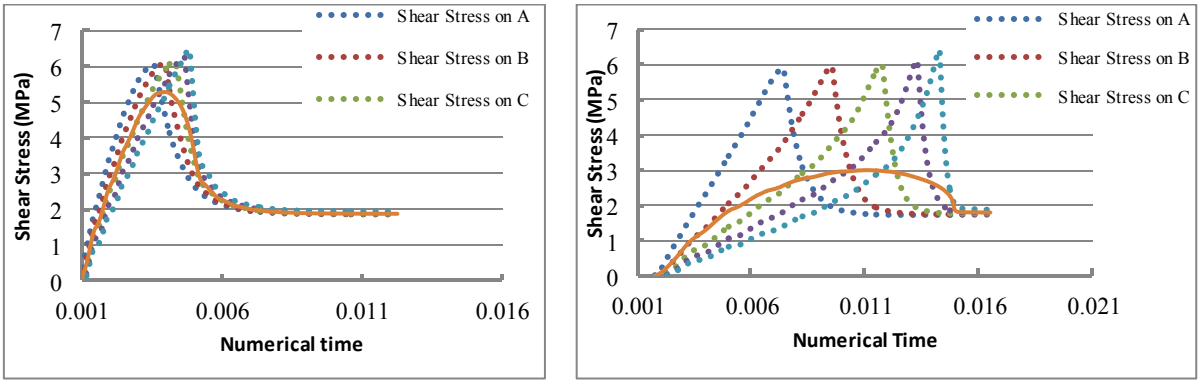

a) b)

Figure 3: Evolution of slip as function of time at different control point for stiff and soft loading systems. a) Shear failure localization for the stiffer system with Young's modulus of 10 GPa. b) Shear failure localization for the softer system with Young's modulus of 1 GPa.

With the understanding and confidence gained through studying the energy terms, mesh size and shear localization in a shear slip, the behavior of a fault in a more realistic setting can be investigated.

4. MODELING A FINITE FAULT

This section simulates a finite fault subjected to an incremental shear loading. Figure 4 shows the model configuration and loading conditions. Model is vertically loaded to 20 MPa and then the horizontal and vertical boundaries are fixed in x and y

directions, respectively. The throughgoing fault is loaded by the coupled horizontal stresses at the center and the model boundaries are located far enough from the loading points so that the fixity of the two ends of the fault has a minimum effect on the results. The adopted loading condition minimizes the nonuniform normal stress concentration on the fault allowing a rather unbiased study on the triggering role of injection into the fault. The injection domain and the quest line specified in this Figure are discussed in the next sections of this paper.

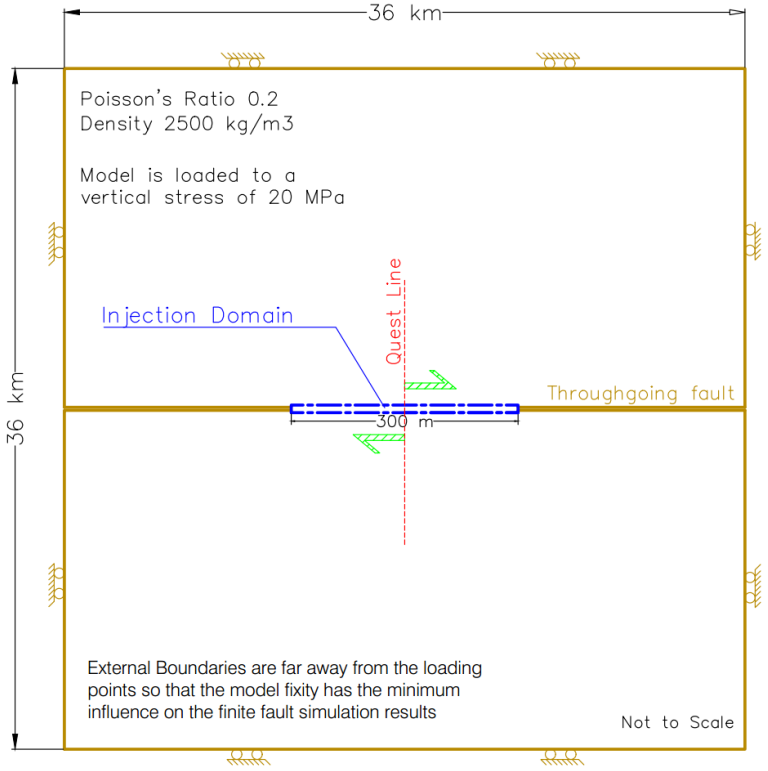

Figure 4: Numerical model geometry and initial conditions.

The coupled stresses acting on the fault are increased gradually from zero to a point at which the average shear stress approaches 6.2 MPa and slip occurs. The coupled stresses are then kept constant until the model reaches equilibrium. The average stress and displacement measurements are calculated over a 300 m long section, centered in the middle of the fault. Considering there is no exact solution to confirm the UDEC energy calculation for this model, this section examines the expected trend of instability for three cases of fault responses under shear stresses: ductile, semi-brittle, and highly brittle faults. The geomechanical properties of these three joint constitutive models are indicated in Table 3.

Table 3. Mechanical properties of the simulated faults

Term	Value		
	Ductile	**Semi-Brittle**	**Highly Brittle**
Joint Constitutive Model	Mohr Coulomb Elastoplastic (MC)	Continuously Yielding	Continuously Yielding
Joint normal stiffness (GPa/m)	50	50	50
Joint shear stiffness (GPa/m)	50	50	50
Joint basic friction angle (degree)	-	7	5
Joint initial friction angle (degree)	17.2	34	34
Joint roughness parameter (mm)	-	0.1	0.1
Cohesion (MPa)	0	0	0

Figure 5 suggests the average shear stress versus average shear displacement curves for the three cases. According to Figure 5, the final values of the relative displacements of the fault planes vary between the three fault behaviors. For the highly brittle fault, the driving force for slip is not the coupled stresses that are constantly applied; rather, the accumulated strain energy in the blocks supports the slip along with releasing some seismic energy. For the case of the ductile fault, the slip does not self-propagate. That is, additional forces are required to maintain a constant shear displacement and as the coupled stresses are maintained constant after the slip initiation, the ductile fault offers the lowest final value for the shear displacement.

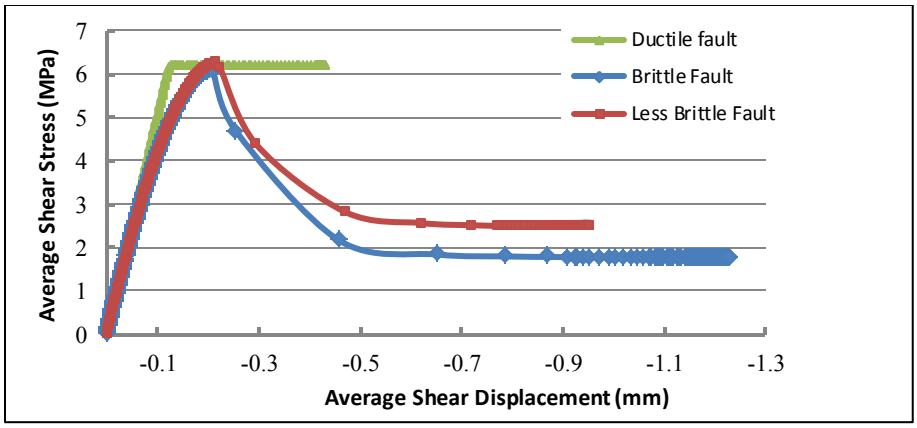

Figure 5: Average shear stress versus average shear displacement along the 300-meter length of the fault (m)

Figure 6a graphs the calculated seismic energy for each case showing that the greatest magnitude for a seismic event originates from a highly brittle fault, consistent with the discussion in section 3.1. Young's modulus for the surrounding rock at all cases is 10Gpa. Figure 6b outlines the effects of loading stiffness on the magnitude of the seismic energy released as a result of a highly brittle slip. As mentioned before, Young's modulus of the rock surrounding the fault is one of the elements dictating the loading stiffness.

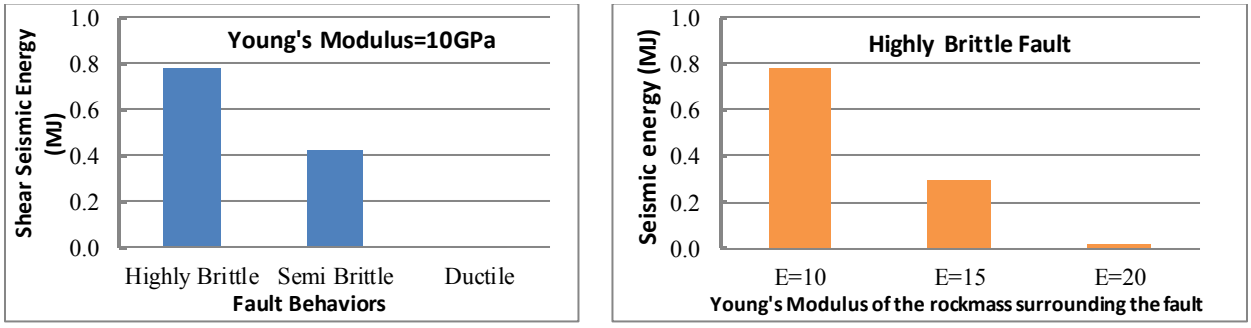

Figure 6: Role of (a) brittleness and (b) loading stiffness in the magnitude of seismic energy

In other words, the magnitude of the interseismic strain depends on the loading stiffness. The interseismic accumulation also correlates with the magnitude of the stored strain energy that feed the released seismic energy. Figure 6b satisfies the expected trend of decreasing the seismic energy as the loading system stiffens. Another way of assessing the results of the developed numerical methodology is through the Elastic Rebound theory.

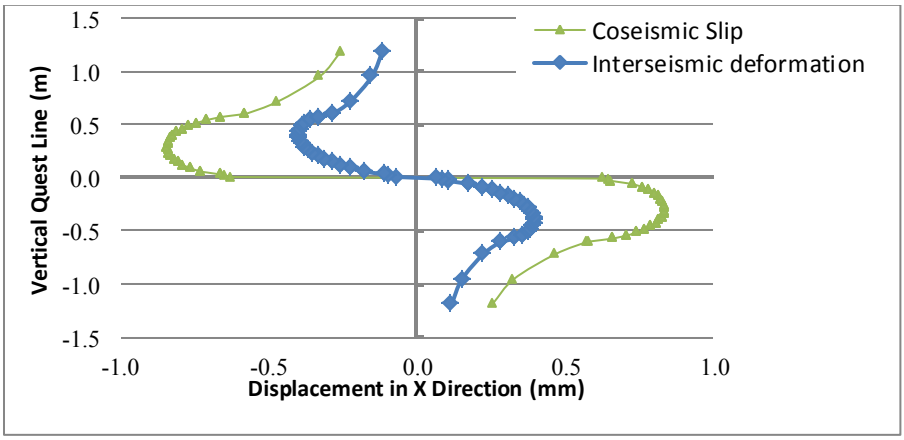

Figure 7: Interseismic deformation and coseismic displacement before and after a seismic event. Displacements are recorded perpendicular to the quest line.

Reid (1910) concluded that an elastic rebound of previously stored elastic strain energy governs seismic events (Reid 1910). Figure 7 reveals the horizontal displacements recorded along the quest line shown in Figure 4. The continuous (interseismic) and discontinuous (coseismic) displacements occur before and after slip of the highly brittle fault, respectively. Interseismic deformation accumulates slowly and is eventually released in a seismic event through coseismic slip.

4.1 Injection-Induced Earthquakes

This paper has thus far developed a methodology to model unstable shear slips and confirmed validity of the results. The next section takes over the pre-slip loaded models and studies seismicity triggered by injecting fluid into a loaded fault. This section investigates the deconfinement of a fault due to the injection pressure. Deconfining a fault can occur due to a wide variety of geological events. In the scope of injection into a fault surrounded by an impermeable continuum, the injection pressure is one of the major causes of deconfinement. This section studies the deconfining effects of injection in both ductile and brittle faults simulated by MC and CY joint models in UDEC, respectively. The matrix is assumed impermeable and fluid pressure is only considered within the fault zone. Here, the role of fault orientation is also examined. Orientation of faults has been proposed as one of the elements contributing to the instability of a slip (Zoback et al. 2012). A fault that is not oriented in favor of a shear slip, with respect to orientations of the principal stresses, is called a misoriented fault while critically stressed faults are referred to as well-oriented faults. Zoback et al. 2012 conducted research on the mechanism of aseismic shear slips during hydraulic fracturing stimulation and concluded that injection-induced slip on a well-oriented fault can propagate rapidly and generate seismic waves whereas the shear slip on misoriented plates can only propagate gradually, depending on the rate of injection. That is, slip can grow along a misoriented fault only as rapidly as pore pressure migrates along it (Zoback et al. 2012). We examine both well-oriented and misoriented faults subject to injection pressure. The radiated seismic energy will be calculated for each model and will be used to evaluate the relative magnitudes of instability for the given conditions. Here, injection is not simulated as transient fluid flow into a fault; instead, a pressure loading is applied in small incremental steps onto the fault plane mimicking the quasi-static pressure increment at different stages of injection. Two target injection pressures are defined for two cases of well-oriented and misoriented faults. Effects of the rate of the pressure changes on the magnitude of seismic energy are studied by four injection patterns each of which gets to the target pressure through different number of increments. After increasing the simulated fluid pressure at each increment, the model is allowed to reach equilibrium. This modeling approach simulates injection pressure changes in an EGS field with the assumption that the time lapse between cycles of changing the down-hole pressure is so long that the stresses around the fault are allowed to reach the steady state. It is assumed that after each increment, the rates at injection and production wells are balanced in such a way that the fluid pressure inside the fault stays constant until the model reaches equilibrium.

4.2 Well-oriented faults

A ductile and brittle fault is loaded to their peak shear strength for simulating well-oriented faults. The effects of injection on instability of ductile and brittle faults are then investigated. A target of 10 MPa injection pressure is defined and four injection scenarios are studied: increasing the injection pressure by 10 MPa (in one sudden increment), 5 MPa (2 increments), 1 MPa (10 increments), and 0.5 MPa (20 increments).

4.2.1 Perfectly ductile fault

The fault initially is loaded to a shear stress of 6.1 MPa, just below the peak average shear strength of 6.2 MPa. The model configuration and loading conditions follow Figure 4 and the fault mechanical properties list in Table 3. Equation 3 shows the role of fluid injection pressure in the shear strength of a ductile fault.

$$\tau_s = (\sigma_n - P_p) \times \tan(\varphi), \qquad (3)$$

where τ_s represents the maximum strength of the fault, σ_n is the normal stress acting on the fault, P_p stands for the injection pressure inside the fault, and φ is the friction angle of the fault planes.

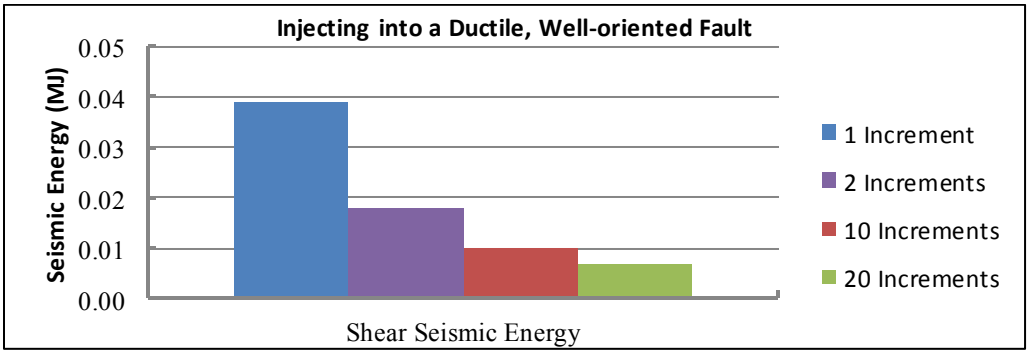

Figure 8: Role of pressure change rate in the magnitude of a shear seismic event along a ductile fault

Increasing the injection pressure decreases the confinement on the fault resulting in a decline in the fault shear strength. Figure 8 shows that gradually reaching the target injection pressure largely suppresses the kinetic energy. However, if injection is applied rapidly to a ductile fault, then the fault may undergo rapid sliding in a manner similar to slip-weakening behavior during a more classically recognized unstable slip event. Therefore, rate of pressure increase, the number of increments by which the fluid pressure inside the fault gets to the target, can turn an aseismic slip to a seismic event along a ductile fault.

4.2.2 Highly Brittle faults

This section employs the highly brittle fault which is critically loaded to a shear stress of 6.1MPa. Figure 9 suggests the role of pressure increase rate in the magnitude of seismic energy once instability appears. The magnitude of the seismic energy correlates with the number of increments, following the same trend as Figure 8. However, compared to the seismic energy released for the case of the ductile fault, Figure 9 suggests greater-magnitude events.

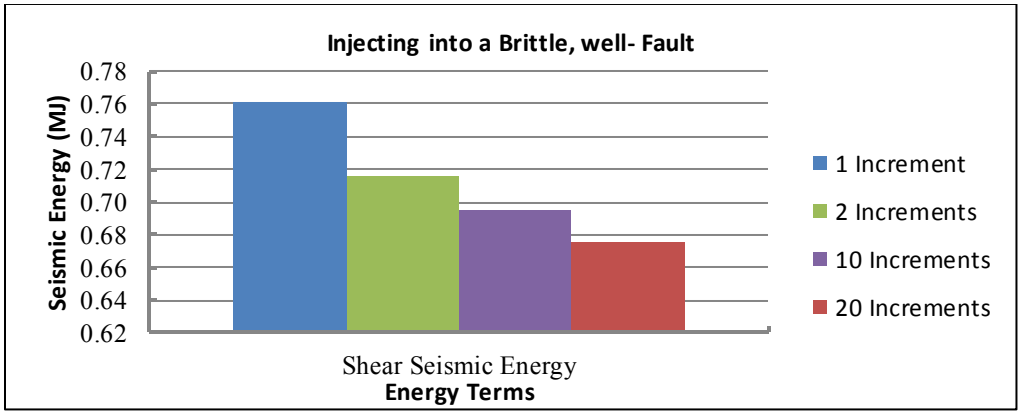

Figure 9: Role of pressure built-up rate on the magnitude of a shear seismic event along a brittle fault

4.3 Misoriented faults

This section simulates a misoriented, highly brittle fault by reducing the pre-slip shear stresses on the brittle fault to 4.3 MPa, 70% of its peak shear strength. As a result, a higher level of deconfinement is needed to trigger a shear slip. The target injection pressure is 18 MPa.

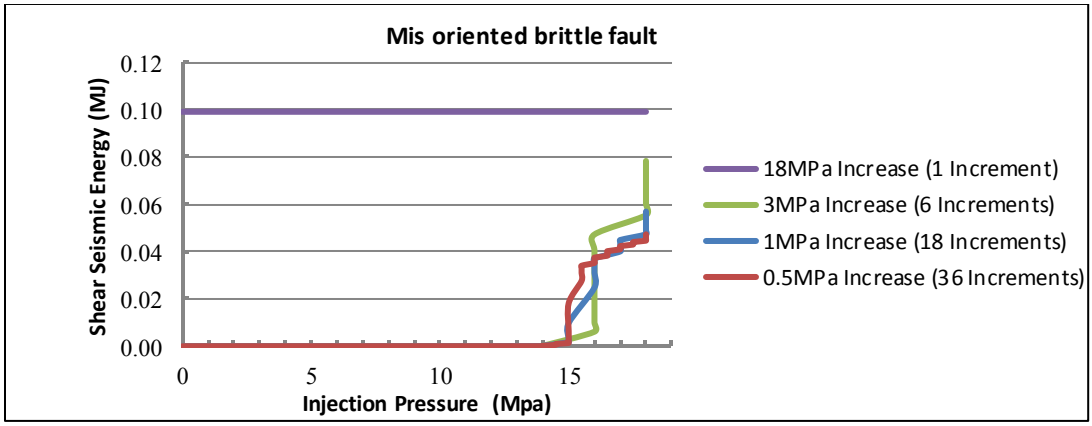

Figure 10: The effects of pressure change rate on the magnitude of the resultant seismic event

Figure 10 shows the magnitude of the seismic energy as injection pressure increases in the four injection patterns: increasing the injection pressure by 18 MPa (one increment), 3 MPa (six increments), 1 MPa (eighteen increments), and 0.5 MPa. Except for the scenario where the injection pressure suddenly increases to 18MPa, the fault withstands a high value of injection pressure of 15 MPa before slip; however, as the shear strength approaches the shear stresses acting on the fault, slip occurs. Once slip initiates, its stability depends on the brittleness of the fault, the number of pressure increments, and the magnitude of the strain energy that has been stored in the rock masses surrounding the fault. Rate of pressure increase does not affect the resulting seismic energy as long as the shear stress does not exceed the shear strength of the fault. After slip initiates, the pressure change rate comes into effect and increases the radiated seismic energy caused by the unstable slip of the brittle fault. Therefore, a misoriented fault can still produce a seismic event since stability of the failure can be dominated by parameters that may override

the stabilizing effects of fault orientations. The maximum shear seismic energy along a misoriented fault in Figure 10 is about seven orders of magnitude less than that of a well-oriented fault in Figure 9. This inconsistency tracks back to the value of the interseismic accumulation. In the misoriented fault, less strain energy is stored in the rock as the fault is not fully loaded to its maximum shear strength.

5. CONCLUSION

An energy-based numerical methodology is developed to identify induced seismic events and estimate the magnitude of these forms of unstable slips. The methodology was examined by graphical calculation of energy terms in a numerical direct shear test and by studying the trend of changing the seismic energy in a slip along a finite fault with different brittle responses. Injection-induced seismicity was then simulated with different injection scenarios. For each model, we calculate the radiated seismic energy from the total kinetic energy released during failure and evaluate the relative magnitudes of instability for the given conditions. The results show that for the case of a well-oriented fault, rapid increase of fluid pressure within a fault induces a self-propagating and unstable slip for the case of the ductile fault. However, the magnitude of the radiated seismic energy increases dramatically with more brittle failure characteristics assigned to the discontinuity. Misoriented faults were also modeled by changing the far-field stress conditions. We showed that unstable slip can occur along a misoriented fault provided the conditions for instability emerge. There is a pore pressure threshold under which the rate of increasing injection pressure does not influence seismicity. This paper confirmed that the developed methodology can identify induced seismic events and directly calculate their radiated seismic energy, or total release of kinetic energy. The energy based methodology can be used to study the conditions required for maintaining an injection rate and resultant downhole pressure below acceptable limits to mitigate the risks associated with large seismic slip. However, further studies are still required to quantitatively account for the effects of other elements, including the change in the rock temperature and pore pressure on the magnitude of an induced seismic event.

REFERENCES

Anderson, P., Fleck, N. A. (1990). "Localization of Plastic Deformation in Shear due to Microcracks." Journal of the Mechanics and Physics of Solids 38(5): 681-699.

Bakhsh, K. J., Nakagawa, M., Bakhsh. K., and Mahmood Arshad et al. (2016). Modeling Thermal Breakthrough in Sedimentary Geothermal System, using COMSOL multiphysics, Stanford, CA: Stanfrod University.

Bakhsh, K. J., Nakagawa, M., Mahmood Arshad, and Lucilia Dunnington (2016). Transport Mechanisms within Thermally-Shocked Region of an Enhanced Geothermal System (EGS). GRC Transactions, Vol. 40.

Evans, K. F., Zappone. A., Kraft, T., Deichmann, N., Moia, F. (2012). "A Survey of the Induced Seismic Responses to Fluid Injection in Geothermal and CO 2 Reservoirs in Europe" Geothermics 41: 30-54.

Garvey, R. and U. Ozbay (2013). Assessing Coal Bumps from Excess Energy in Finite Difference Models. Proceedings of the 32nd International Conference on Ground Control in Mining. Morgantown, WV.

Gu, R. and U. Ozbay (2015). "Numerical Investigation of Unstable Rock Failure in Underground Mining Condition." Computers and Geotechnics 63: 171-182.

Nakagawa, M., Bakhsh. K., and Mahmood Arshad. 2016. “Beyond Hydrocarbon Extraction: Enhanced Geothermal Systems.” In New Frontiers in Oil and Gas Exploration, 487–506. Cham: Springer International Publishing.

Nakagawa, M., Bakhsh, K., and Mahmood Arshad. 2016. “Beyond Hydrocarbon Extraction: Enhanced Geothermal Systems.” In New Frontiers in Oil and Gas Exploration, 487–506. Cham: Springer International Publishing. doi:10.1007/978-3-319-40124-9_15 Jin, C. and G. Cusatis (2016). New frontiers in oil and gas exploration, Springer.

Karimi, S. and Kazemi, H. (2015). Capillary Pressure Measurement using Reservoir Fluids in a Middle Bakken Core. SPE Western Regional Meeting, Society of Petroleum Engineers.

Karimi, S and Kazemi, H. (2016). Experimental Study of the Effect of Core Aging on Fluid Distribution in Middle Bakken Cores. SPE Low Perm Symposium, Society of Petroleum Engineers.

Karimi, S., Saidian. M., Parsad, M., Kazemi, H. (2015). Reservoir Rock Characterization using Centrifuge and Nuclear Magnetic Resonance: A laboratory study of middle bakken cores. SPE Annual Technical Conference and Exhibition, Society of Petroleum Engineers.

Khademian, Z., Poeck, E., Garvey, R., Ozbay, U. (2016). Studies of Seismicity Generated by Unstable Failures around Circular Excavations. 50th US Rock Mechanics/Geomechanics Symposium, American Rock Mechanics Association.

Khademian, Z., Shahriar, K., Nik, M. G. (2012). "Developing an Algorithm to Estimate In-situ Stresses using a Hybrid Numerical Method based on Local Stress Measurement." International Journal of Rock Mechanics and Mining Sciences 55: 80-85.

McClure, M. W. and R. N. Horne (2011). "Investigation of Injection-Induced Seismicity using a Coupled Fluid Flow and Rate/State Friction Model." Geophysics 76(6): WC181-WC198.

Poeck, E., Khademian, Z., Garvey, R., Ozbay, U.. (2016). Modeling Unstable Rock Failures in Underground Excavations. Rock Mechanics and Rock Engineering: From the Past to the Future, CRC Press: 505-509.

Reid, H. (1910). "The Mechanics of the Earthquake: The California Earthquake of April 18, 1906, report, vol. 2, 192 pp." State Earthquake Invest. Comm., Carnegie Inst. of Wash., Washington, DC.

Rice, J. R. (1983). "Constitutive Relations for Fault Slip and Earthquake Instabilities." Pure and applied geophysics 121(3): 443-475.

Rutqvist, J., Rinaldi, A. P., Cappa, F., Moridis, G. (2013). "Modeling of Fault Reactivation and Induced Seismicity during Hydraulic Fracturing of Shale-Gas Reservoirs." Journal of Petroleum Science and Engineering 107: 31-44.

Salamon, M. (1984). "Energy Considerations in Rock Mechanics: fundamental results." Journal of the South African Institute of Mining and Metallurgy 84(8): 233-246.

Zhang, Y., Person, M., Rupp, J., Ellett, K., Celia, M. A., Gable, C. W., Bown, B., Evens, J., Bandilla, K., Mozley, P., Dewers, T., Elliot, T. (2013). "Hydrogeologic Controls on Induced Seismicity in Crystalline Basement Rocks due to Fluid Injection into Basal Reservoirs." Groundwater 51(4): 525-538.

Zoback, M. D.,Kohli, A., Das, I., McClure, M. (2012). The Importance of Slow Slip on Faults during Hydraulic Fracturing Stimulation of Shale Gas Reservoirs. SPE Americas Unconventional Resources Conference, Society of Petroleum Engineers.